

Systematic errors in current quantum state tomography tools

Christian Schwemmer,^{1,2} Lukas Knips,^{1,2} Daniel Richart,^{1,2} and Harald Weinfurter^{1,2}
¹Max-Planck-Institut für Quantenoptik, Hans-Kopfermann-Str. 1, D-85748 Garching, Germany and
²Department für Physik, Ludwig-Maximilians-Universität, D-80797 München, Germany

Tobias Moroder,³ Matthias Kleinmann,³ and Otfried Gühne,³
³Naturwissenschaftlich-Technische Fakultät, Universität Siegen, Walter-Flex-Str. 3, D-57068 Siegen, Germany

Common tools for obtaining physical density matrices in experimental quantum state tomography are shown here to cause systematic errors. For example, using maximum likelihood or least squares optimization for state reconstruction, we observe a systematic underestimation of the fidelity and an overestimation of entanglement. A solution for this problem can be achieved by a linear evaluation of the data yielding reliable and computational simple bounds including error bars.

PACS numbers: 03.65.Ud, 03.65.Wj, 06.20.Dk

Introduction.—Quantum state tomography (QST) [1] enables us to fully determine the state of a quantum system and thereby to deduce all its properties. As such QST is widely used to characterize and to evaluate numerous experimentally implemented qubit states or their dynamics, e.g., in ion trap experiments [2, 3], photonic systems [4, 5], superconducting circuits [6], or nuclear magnetic resonance systems [7, 8]. The increasing complexity of today's multiqubit/qudit quantum systems brought new challenges but also progress. Now, highly efficient methods allow an even scalable analysis for important subclasses of states [9, 10]. The calculation of errors of QST was significantly improved although the errors remain numerically expensive to evaluate for larger systems [11]. Moreover QST was used to detect systematic errors in the alignment of an experiment itself [12].

A central step in QST is to establish the state from the acquired experimental data. A direct, linear evaluation of the data returns almost for sure an unphysical density matrix with negative eigenvalues [13]. Thus, several schemes have been developed to obtain a physical state which resembles the observed data as closely as possible [4, 14, 15].

In this Letter we test whether the naïve expectation is met that QST delivers proper estimates for physical quantities. We test this for the two most commonly used reconstruction schemes—maximum likelihood (ML) [15] and least squares (LS) [4]—using Monte Carlo simulations. This expectation is not fulfilled: both schemes return states which deviate systematically from the true state, e.g., underestimate the fidelity as shown in Fig. 1. For data sizes typical in multiqubit experiments the deviation from the true value is significant, in fact it is larger than commonly deduced “error bars” [16]. We show that the constraint of physicality necessarily leads to systematic errors for the reconstruction scheme. The size of these errors depends on the experimental noise and unavoidable statistical fluctuations. We find that it is advisable to evaluate linear operators directly on the raw data. We also show how physical quantities that

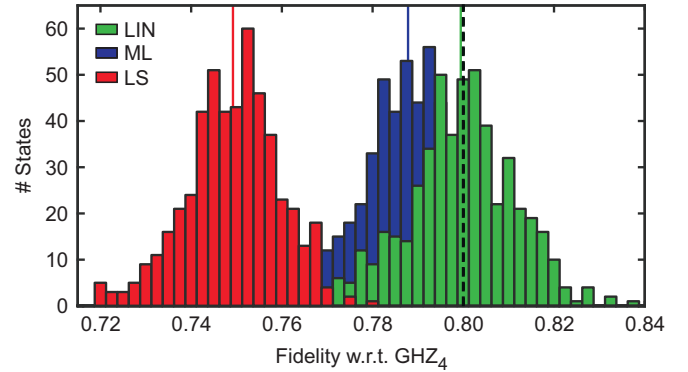


FIG. 1: (Color online) Histogram of the fidelity estimates of 500 independent simulations of QST of a noisy four-party Greenberger-Horne-Zeilinger (GHZ) state for three different reconstruction schemes. The values obtained via maximum likelihood (ML, blue) or least squares (LS, red) fluctuate around a value that is lower than the initial fidelity of 80% (dashed line). For comparison, we also show the result using linear inversion (LIN, green), which does not suffer from such a systematic error called bias.

are given by convex (concave) nonlinear functions of the density matrix like the bipartite negativity etc., can be linearized thereby providing a meaningful lower (upper) bound, namely a directly computable error bar.

Standard state tomography tools.—The aim of QST is to identify the initially unknown state ρ_0 of a system via appropriate measurements on multiple preparations of this state. For an n -qubit system, the so-called Pauli tomography scheme consists of measuring in the eigenbases of all 3^n possible combinations of local Pauli operators, each yielding 2^n possible results [4]. In more general terms, in a tomography protocol one repeats for each measurement setting s the experiment a certain number of times N_s and obtains c_r^s times the result r . These numbers then yield the frequencies $f_r^s = c_r^s/N_s$. The probability to observe the outcome r for setting s is given by $P_{\rho_0}^s(r) = \text{tr}(\rho_0 M_r^s)$. Here, M_r^s labels the measurement

operator corresponding to the result r when measuring setting s . The probabilities $P_{\varrho_0}^s(r)$ will uniquely identify the unknown state ϱ_0 , if the set of operators M_r^s spans the space of Hermitian operators.

Provided the data f , i.e., the set of experimentally determined frequencies f_r^s one requires a method to determine the estimate $\hat{\varrho} \equiv \hat{\varrho}(f)$ of the unknown state ϱ_0 . Simply inverting the relations for $P_{\varrho_0}^s(r)$ we obtain

$$\hat{\varrho}_{\text{LIN}} = \sum_{r,s} A_r^s f_r^s \quad (1)$$

where A_r^s are determined from the measurement operators M_r^s [8, 17]. Note that there is a canonical construction of A_r^s even for the case of an overcomplete set of M_r^s , see SM 1. This reconstruction of $\hat{\varrho}_{\text{LIN}}$ is computationally simple and has become known as linear inversion (LIN).

Yet, due to unavoidable statistical fluctuations the estimate $\hat{\varrho}_{\text{LIN}}$ is not a physical density operator for typical experimental situations, i.e., generally some eigenvalues are negative. Besides the issues of a physical interpretation of such a “state” this causes further problems in evaluating interesting functions like the von Neumann entropy, the quantum Fisher information or an entanglement measure like the negativity as these functions are defined or meaningful only for valid, i.e., positive-semidefinite, quantum states.

For this reason, different methods have been introduced that mostly follow the paradigm that the reconstructed state $\hat{\varrho} = \arg \max_{\varrho \geq 0} T(\varrho|f)$ maximizes a target function $T(\varrho|f)$ within the set of *valid* density operators. This target function thereby measures how well a density operator ϱ agrees with the observed data f . Two common choices are maximum likelihood (ML) [15] where $T_{\text{ML}} = \sum_{r,s} f_r^s \log[P_{\varrho}^s(r)]$, and least squares (LS) [4] where $T_{\text{LS}} = -\sum_{r,s} [f_r^s - P_{\varrho}^s(r)]^2 / P_{\varrho}^s(r)$. We denote the respective solutions by $\hat{\varrho}_{\text{ML}}$ and $\hat{\varrho}_{\text{LS}}$. From these estimates one then easily computes any physical quantity of the observed state, like e.g. the fidelities $\hat{F}_{\text{ML}} = \langle \psi | \hat{\varrho}_{\text{ML}} | \psi \rangle$ and $\hat{F}_{\text{LS}} = \langle \psi | \hat{\varrho}_{\text{LS}} | \psi \rangle$ with respect to the target state $|\psi\rangle$.

Numerical simulations.—To enable detailed analysis of the particular features of the respective state reconstruction algorithm and to exclude influence of systematic experimental errors we perform Monte Carlo simulations. For a chosen state ϱ_0 the following procedure is used: *i*) Compute the single event probabilities $P_{\varrho_0}^s(r)$, *ii*) toss a set of frequencies according to a multinomial distribution, *iii*) reconstruct the state with either reconstruction method and compute the functions of interest, *iv*) carry out steps *ii*) and *iii*) 500 times. Note that the optimality of the maximizations for ML and LS in step (ii) is certified by convex optimization [10, 18].

Exemplarily, we first consider the four-qubit Greenberger-Horne-Zeilinger (GHZ) state

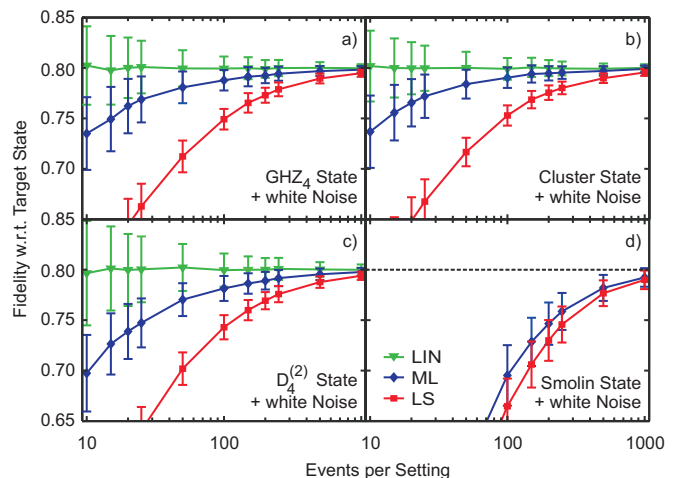


FIG. 2: (Color online) The performance of ML, LS, and LIN methods depending on the number of events N_s per setting and for four different noisy initial states ϱ_0 . Note that the fidelity can only be calculated linearly if the reference state is pure which is not the case for the Smolin state [19]. Therefore only the curves for ML and LS are plotted for the Smolin state.

$|\text{GHZ}_4\rangle = (|0000\rangle + |1111\rangle)/\sqrt{2}$ mixed with white noise, i.e., $\varrho_0 = p|\text{GHZ}_4\rangle\langle\text{GHZ}_4| + (1-p)\mathbb{1}/16$ where p is chosen such that the fidelity is $\langle\text{GHZ}_4|\varrho_0|\text{GHZ}_4\rangle = 0.8$. This state is used to simulate the Pauli tomography scheme. Fig. 1 shows an exemplary histogram of the resulting fidelities for $N_s = 100$ measurement repetitions which is a typical value used for various multiqubit experiments. The fidelities obtained via LIN reconstruction fluctuate around the initial value ($\bar{F}_{\text{LIN}} = 0.799 \pm 0.012$). (The values given there are the mean and the standard deviation obtained from the 500 reconstructed states). In stark contrast, both ML ($\bar{F}_{\text{ML}} = 0.788 \pm 0.010$) and even worse LS ($\bar{F}_{\text{LS}} = 0.749 \pm 0.010$) systematically underestimate the fidelity, i.e., are strongly biased. Evidently, the fidelities of the reconstructed states differ by more than one standard deviation for ML and even more than five standard deviations for LS. The question arises how these systematic errors depend on the parameters of the simulation. Let us start by investigating the dependence on the number of repetitions N_s . Fig. 2a shows the mean and the standard deviations of histograms like the one shown in Fig. 1. for different N_s . As expected, the systematic errors are more profound for low number of repetitions N_s per setting s and decrease with increasing N_s . Yet, even for $N_s = 500$, a number hardly used in multiqubit experiments, \bar{F}_{LS} still deviates by one standard deviation from the correct value. The effect is also by no means special for the GHZ state but was equally observed for other prominent four-party states, here also chosen with a true fidelity of 80%, see Fig. 2b-2d and the Supplemental Material (SM).

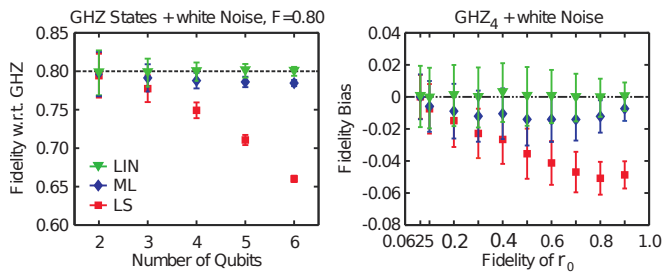


FIG. 3: (Color online) The behavior of ML, LS, and LIN depending on the number of qubits n (left) and the fidelity of ϱ_0 (right).

The systematic deviations vary also with the number of qubits or the purity of the initial state. Fig. 3a shows the respective dependencies of the fidelity for n -qubit states $\varrho_0 = p|\text{GHZ}_n\rangle\langle\text{GHZ}_n| + (1-p)\mathbb{1}/2^n$ (for $N_s = 100$). Here, a significant increase of the bias with the number of qubits is observed especially for LS. Also when varying the purity or fidelity with the GHZ state, respectively, we observe a remarkable deviation for ML and LS estimators (Fig. 3b). If the initial fidelity is very low, the effect is negligible, but large fidelity values suffer from stronger deviations, especially for LS.

The commonly specified “error bars” used in QST quantify the statistical fluctuations of the estimate $\hat{\varrho}$. Starting either from the estimate $\hat{\varrho}_{\text{EST}}$ ($\text{EST} \in \{\text{ML}, \text{LS}\}$) or the observed data set f this error is typically accessed by Monte Carlo sampling: One repeatedly simulates data sets $f^{(i)}$ according to the state ϱ_{EST} or f together with a representative noise model for the respective experiment and reconstructs the state $\hat{\varrho}(f^{(i)})$. From the resulting empirical distribution, one then reports the standard deviation (or a region including, say, 68% of the simulated states) for the matrix elements or for quantities of interest [16], see also SM 3. However, the problem with such error bars is that they might be too small since they reflect only statistical fluctuations of the measured frequencies, but not the systematic error which easily can be larger [20].

In summary, we observe systematic errors, which depend on the state reconstruction method and the strength of the statistical fluctuations of the count rates shown here as dependence on the number of repetitions of the experiment. Since the effect even depends on the unknown initial state any manual correction of the bias is unjustifiable. Let us emphasize that in most cases the initial value differs by more than the “error bar” determined via bootstrapping (cf. SM 3).

Biased and unbiased estimators.—The systematic offset discussed above is well-known in the theory of point estimates [20]. Expressed for QST, an estimator $\hat{\varrho}$ is called unbiased if its fluctuations are centered around the

true mean, such that for its expectation value

$$\mathbb{E}_{\varrho_0}(\hat{\varrho}) \equiv \sum_f P_{\varrho_0}(f) \hat{\varrho}(f) = \varrho_0 \quad (2)$$

holds for all possible states ϱ_0 with $P_{\varrho_0}(f)$ the probability to observe the data f . An estimator that violates Eq. (2) is called biased. Similar definitions hold for instance for fidelity estimators, $\mathbb{E}_{\varrho_0}(\hat{F}) = \langle \psi | \varrho_0 | \psi \rangle \equiv F_0$. This terminology is motivated by the form of the mean squared error, which decomposes for example for the fidelity into

$$\mathbb{E}_{\varrho_0}[(\hat{F} - F_0)^2] = \mathbb{V}_{\varrho_0}(\hat{F}) + [\mathbb{E}_{\varrho_0}(\hat{F}) - F_0]^2, \quad (3)$$

where $\mathbb{V}(\hat{F}) \equiv \mathbb{E}(\hat{F}^2) - \mathbb{E}(\hat{F})^2$ denotes the variance. Equation (3) consists of two conceptually different parts. The first being a statistical term quantifying the fluctuations of the estimator \hat{F} itself. The second, purely systematic term, is called *bias* and vanishes for unbiased estimators [21]. Note that, since the expectation values of the frequencies are the probabilities, $\mathbb{E}_{\varrho_0}(f_r^s) = P_{\varrho_0}^s(r)$, and because $\hat{\varrho}_{\text{LIN}}$ as given by Eq. (1) is linear in f_r^s the determination of a quantum state using LIN is unbiased. However, as shown below, for QST the bias is inherent to estimators constraint to giving only physical answers.

Proposition. *A reconstruction scheme for QST that always yields valid density operators is biased.*

Proof. For a tomography experiment on the state $|\psi_i\rangle$ with finite measurement time there is a set of possible data $\mathcal{S}_i = \{f_i | P_{|\psi_i\rangle}(f_i) > 0\}$, with $P_{|\psi_i\rangle}(f_i)$ the probability to obtain data f_i when observing state $|\psi_i\rangle$.

Consider two pure non-orthogonal states $|\psi_1\rangle$ and $|\psi_2\rangle$ ($\langle \psi_1 | \psi_2 \rangle \neq 0$). For these two states there exists a non-empty set of data $\mathcal{S}_{12} = \{f' | P_{|\psi_1\rangle}(f') \cdot P_{|\psi_2\rangle}(f') > 0\} = \mathcal{S}_1 \cap \mathcal{S}_2$, which can occur for both states.

Now let us assume that a reconstruction scheme $\hat{\varrho}$ provides a valid quantum state $\hat{\varrho}(f)$ for all possible outcomes f and that Eq. (2) is satisfied for $|\psi_1\rangle$, i.e., $\sum_{\mathcal{S}_1} P_{|\psi_1\rangle}(f_1) \hat{\varrho}(f_1) = |\psi_1\rangle\langle\psi_1|$. This incoherent sum over all $\hat{\varrho}(f_1)$ can be equal to the pure state $|\psi_1\rangle\langle\psi_1|$ only for the (already pathological) case that $\hat{\varrho}(f_1) = |\psi_1\rangle\langle\psi_1|$ for all $f_1 \in \mathcal{S}_1$. This means that the outcome of the reconstruction is fixed for all f_1 including all data $f' \in \mathcal{S}_{12}$. As these data also occur for state $|\psi_2\rangle$ there exist $f_2 \in \mathcal{S}_{12}$ with $\hat{\varrho}(f_2) = |\psi_1\rangle\langle\psi_1| \neq |\psi_2\rangle\langle\psi_2|$. Thus, in Eq. (2), the sum over all reconstructed states now is an incoherent mixture of at least two pure states and the condition $\sum_{\mathcal{S}_2} P_{|\psi_2\rangle}(f_2) \hat{\varrho}(f_2) = |\psi_2\rangle\langle\psi_2|$ is violated for $|\psi_2\rangle$. Hence, $\hat{\varrho}$ does not obey Eq. (2) for $|\psi_2\rangle$ and is therefore biased [22]. \square

This leaves us with the trade-off: Should one necessarily use an algorithm like ML or LS to obtain a valid quantum state but suffer from a bias, or should one use LIN which is unbiased but typically delivers an unphysical result?

Parameter estimation by linear evaluation.—Here, we demonstrate that starting from $\hat{\rho}_{\text{LIN}}$ it is straightforward to provide a valid, lower/upper bound and an easily computable confidence region for many quantities of interest. For that we exploit the fact that many relevant functions are either convex, like most entanglement measures or the quantum Fisher information, or concave, like the von Neumann entropy. We linearize these operators around some properly chosen state in order to obtain a reliable lower (upper) bound. Note that typically a lower bound on an entanglement measure is often suited for evaluating experimental states whereas an upper bound does not give much additional information.

Recall that a differentiable function $g(x)$ is convex if $g(x) \geq g(x') + \nabla g(x')^T(x - x')$ holds for all x, x' . In our case we are interested in a function $g(x) = g[\varrho(x)]$ where x is a variable to parametrize a quantum state ϱ in a linear way. From convexity it follows that it is possible to find an operator L , such that

$$\text{tr}(\varrho_0 L) \leq g(\varrho_0) \quad (4)$$

holds for all ϱ_0 (similarly an upper bound is obtained for concave functions). This operator can be determined from the derivatives of $g(x)$ with respect to x at a suitable point x' . For cases where the derivative is hard to compute such an operator can also be obtained from the Legendre transformation [23] or directly inferred from the definition of the function $g(x)$ [24]. A detailed discussion is given in the SM 5.

For this bound a confidence region, i.e., the error bars in the frequentistic approach, can be calculated. For example a one-sided confidence region of level γ can be described by a function \hat{C} on the data f such that $\text{Prob}_{\varrho_0}[\hat{C} \leq g(\varrho_0)] \geq \gamma$ holds for all ϱ_0 [20]. According to Hoeffding's tail inequality [25] and a given decomposition of $L = \sum_r l_r^s M_r^s$ into the measurement operators M_r^s a confidence region then is given by

$$\hat{C} = \text{tr}(\hat{\rho}_{\text{LIN}} L) - \sqrt{\frac{h^2 |\log(1 - \gamma)|}{2N_s}}, \quad (5)$$

where h^2 is given by $h^2 = \sum_s (l_{\text{max}}^s - l_{\text{min}}^s)^2$, and $l_{\text{max/min}}^s$ denotes the respective extrema of l_r^s over r for each setting s . Although not being optimal, such error bars are easy to evaluate and valid without extra assumptions. Since we directly compute a confidence interval on $g(x)$ this is also generally a tighter error bar than those deduced from a “smallest” confidence region on density operators which tend to drastically overestimate the error (see SM 4 for an example).

In the following we show how to use a linearized operator on the example of the bipartite negativity [24]. (For the quantum Fisher information [26] and additional discussion see SM 5.) A lower bound on the negativity

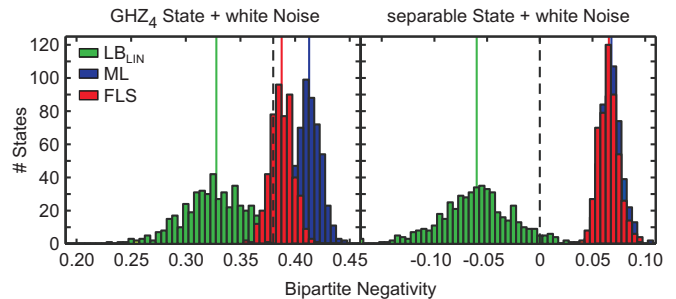


FIG. 4: (Color online) Lower bound LB_{LIN} obtained by linearizing bipartite negativity for a four-qubit product (left) and the GHZ state (right) both mixed with white noise resulting in 80% fidelity. The ML and LS reconstruction leads to a systematic overestimation of the negativity, while the lower bound yields a valid estimate.

$N(\varrho_{AB})$ of a bipartite state ϱ_{AB} is given by

$$N(\varrho_{AB}) \geq \text{tr}(\varrho_{AB} L) \quad (6)$$

for any L satisfying $\mathbb{1} \geq L^{T_A} \geq 0$, where the superscript T_A denotes partial transposition [27] with respect to party A . The inequality (6) is tight if L is the projector on the negative eigenspace of $\varrho_{AB}^{T_A}$. Using this linear expression one can directly compute the lower bound on the negativity and by using Eq. (5) the one-sided confidence region. Any choice of L is in principle valid, however for a good performance L should be chosen according to the experimental situation. We assume, however, no prior knowledge and rather estimate L by the projector on the negative eigenspace of $\hat{\varrho}_{\text{ML}}^{T_A}$ deduced from an *additional* tomography again with $N_s = 100$ counts per setting. One can, of course, also start with an educated guess of L motivated by the target state one wants to prepare. In any case, in order to apply Eq. (5) and to assure a linear evaluation of the data the operator L must be chosen independently of the tomographic data [12].

Fig. 4 shows the distributions of the negativity between qubits $A = \{1, 2\}$ and $B = \{3, 4\}$ for the four-qubit GHZ state and for the separable four-qubit state $|\psi_{\text{sep}}\rangle \propto (|0\rangle + |+\rangle)^{\otimes 4}$, each mixed with white noise such that the fidelity with the respective pure state is 80%. In both cases we observe that ML and LS *overestimate* the amount of entanglement. Even worse, if no entanglement is present, ML and LS clearly indicate entanglement. In contrast, the lower bound of the negativity, as given by Eq. (6), does not indicate false entanglement.

Conclusion.—Any state reconstruction algorithm enforcing physicality of the result suffers from systematic deviations. We have shown that for the commonly used methods and the typical measurement schemes this bias is significant for data sizes typical in current experiments. It leads to systematically wrong statements about derived quantities like the fidelity or the negativity which can lead to erroneous conclusions particularly for the

presence of entanglement. Equivalent statements can be inferred for process tomography.

We have demonstrated that the simple method of linear inversion can be used to overcome these problems in many cases. Expectation values being linear in ϱ do not exhibit a bias at all even if $\hat{\varrho}_{\text{LIN}}$ is not physical in the overwhelming number of cases. A linearization of convex (concave) nonlinear physical quantities yields meaningful lower (upper) bounds together with easy to calculate confidence intervals restoring the trust in quantum state and process tomography.

We like to thank D. Gross, P. Drummond and M. Raymer for stimulating discussions. This work has been supported by the EU (Marie Curie CIG 293993/ENFOQI and ERC QOLAPS), the BMBF (Chist-Era project QUASAR) and QCCC of the Elite Network of Bavaria.

-
- [1] M. G. A. Paris and J. Řeháček, eds., *Quantum state estimation* (Springer Berlin Heidelberg, 2004).
- [2] H. Häffner, W. Hänsel, C. F. Roos, J. Benhelm, D. Chekalkar, M. Chwalla, T. Körber, U. D. Rapol, M. Riebe, P. O. Schmidt et al., *Nature* **438**, 643 (2005).
- [3] J. P. Home, D. Hanneke, J. D. Jost, J. M. Amini, D. Leibfried, and D. J. Wineland, *Science* **325**, 1227 (2009).
- [4] D. F. V. James, P. G. Kwiat, W. J. Munro, and A. G. White, *Phys. Rev. A* **64**, 052312 (2001).
- [5] K. J. Resch, P. Walther, and A. Zeilinger, *Phys. Rev. Lett.*, **94**, 070402 (2005); N. Kiesel, C. Schmid, G. Tóth, E. Solano, and H. Weinfurter, *Phys. Rev. Lett.* **98**, 063604 (2007); M. W. Mitchell, C. W. Ellenor, S. Schneider, and A. M. Steinberg, *Phys. Rev. Lett.* **91**, 120402 (2003).
- [6] L. DiCarlo, J. M. Chow, J. M. Gambetta, L. S. Bishop, B. R. Johnson, D. I. Schuster, A. Majer, J. Blais, L. Frunzio, S. M. Girvin, and R. J. Schoelkopf, *Nature* **460**, 240 (2009); M. Neeley, R. C. Bialczak, M. Lenander, E. Lucero, M. Mariantoni, A. D. O’Connell, D. Sank, H. Wang, M. Weides, J. Wenner et al., *Nature* **467**, 570 (2010); A. Fedorov, L. Steffen, M. Baur, M. da Silva, and A. Wallraff, *Nature* **481**, 170 (2012).
- [7] O. Mangold, A. Heidebrecht, and M. Mehring, *Phys. Rev. A* **70**, 042307 (2004); M. A. Nielsen, E. Knill, and R. Laflamme, *Nature* **396**, 52 (1998).
- [8] I. L. Chuang and M. A. Nielsen, *J. Mod. Opt.* **44**, 2455 (1997).
- [9] D. Gross, Y.-K. Liu, S. T. Flammia, S. Becker, and J. Eisert, *Phys. Rev. Lett.* **105**, 150401 (2010); G. Tóth, W. Wieczorek, D. Gross, R. Krischek, C. Schwemmer, and H. Weinfurter, *Phys. Rev. Lett.* **105**, 250403 (2010); M. Cramer, M. B. Plenio, S. T. Flammia, D. Gross, S. D. Bartlett, R. Somma, O. Landon-Cardinal, Y.-K. Liu, and D. Poulin, *Nat. Commun.* **1**, 9 (2010); O. Landon-Cardinal and D. Poulin, *New J. Phys.* **14**, 085004 (2012).
- [10] T. Moroder, P. Hyllus, G. Tóth, C. Schwemmer, A. Niggebaum, S. Gaile, O. Gühne, and H. Weinfurter, *New J. Phys.* **14**, 105001 (2012).
- [11] M. Christandl and R. Renner, *Phys. Rev. Lett.* **109**, 120403 (2012); T. Sugiyama, P. S. Turner, and M. Muraö, *Phys. Rev. Lett.* **111**, 160406 (2013); R. Blume-Kohout, arXiv:1202.5270; J. Shang, H. K. Ng, A. Sehwat, X. Li, and B.-G. Englert, *New J. Phys.* **15**, 123026 (2013).
- [12] T. Moroder, M. Kleinmann, P. Schindler, T. Monz, O. Gühne, and R. Blatt, *Phys. Rev. Lett.* **110**, 180401 (2013); D. Rosset, R. Ferretti-Schöbitz, J.-D. Bancal, N. Gisin, and Y.-C. Liang, *Phys. Rev. A* **86**, 062325 (2012); C. Stark, arXiv:1209.5737; N. K. Langford, *New J. Phys.* **15**, 035003 (2013); S. J. van Enk and R. Blume-Kohout, *New J. Phys.* **15**, 025024 (2013).
- [13] D. Smithey, M. Beck, and M. G. Raymer, *Phys. Rev. Lett.* **70**, 1244 (1993); G. M. D’Ariano, C. Macchiavello, and N. Sterpi, *Quantum Semiclass. Opt.* **9**, 929 (1997); U. Leonhardt, M. Munroe, T. Kiss, T. Richter, and M. Raymer, *Opt. Comm.* **127**, 144 (1996).
- [14] R. Blume-Kohout, *New J. Phys.* **12**, 043034 (2010); R. Blume-Kohout, *Phys. Rev. Lett.* **105**, 200504 (2010).
- [15] Z. Hradil, *Phys. Rev. A* **55**, R1561 (1997).
- [16] B. Efron and R. J. Tibshirani, *An introduction to the bootstrap* (Chapman & Hall, 1994).
- [17] J. F. Poyatos and J. I. Cirac, *Phys. Rev. Lett.* **78(2)**, 390 (1997); N. Kiesel, Ph.D. thesis, Ludwig-Maximilians-Universität München (2007); T. Kiesel, *Phys. Rev. A* **85**, 052114 (2012).
- [18] S. Boyd and S. Vandenberghe, *Convex optimization* (Cambridge University Press, 2004).
- [19] J. A. Smolin, *Phys. Rev. A* **63**, 032306 (2001).
- [20] A. F. Mood, *Introduction to the theory of statistics* (McGraw-Hill Inc., 1974).
- [21] It is well-known that estimators can be biased for a finite number of samples or for particular additional conditions and constraints. An example is the estimate of the variance σ^2 of a Gaussian distribution with known mean μ . The ML estimate from N samples x_i gives $\hat{\sigma}_{\text{ML}}^2(x_i) = \frac{1}{N} \sum_i (x_i - \mu)^2$, while an unbiased estimator is $\hat{\sigma}^2(x_i) = \frac{1}{N-1} \sum_i (x_i - \mu)^2$.
- [22] This proof, given here for pure states, can be generalized for mixed states ϱ_1 and ϱ_2 with the ranges of the two states not sharing any vector.
- [23] O. Gühne, M. Reimpell, and R. F. Werner, *Phys. Rev. Lett.* **98**, 110502 (2007); J. Eisert, F. G. S. L. Brandao, and K. M. R. Audenaert, *New J. Phys.* **9**, 46 (2007).
- [24] G. Vidal and R. F. Werner, *Phys. Rev. A* **65**, 032314 (2002).
- [25] M. Tomamichel, C. C. W. Lim, N. Gisin, and R. Renner, *Nat. Commun.* **3**, 634 (2012); S. T. Flammia and Y.-K. Liu, *Phys. Rev. Lett.* **106**, 230501 (2011); M. P. da Silva, O. Landon-Cardinal, and D. Poulin, *Phys. Rev. Lett.* **107**, 210404 (2011).
- [26] D. Petz and C. Ghinea, QP-PQ: Quantum Probab. White Noise Anal. **27**, 261 (2011).
- [27] A. Peres, *Phys. Rev. Lett.* **77**, 1413 (1996).
- [28] R. A. Horn and C. R. Johnson, *Topics in matrix analysis* (Cambridge University Press, 1991).

Supplemental Material

SM 1: Quantum state reconstruction using linear inversion

In [4] it is explained how to obtain the estimate $\hat{\rho}_{\text{LIN}}$ for an n -qubit state from the observed frequencies of a complete set of projection measurements, i.e. 4^n results. Yet, the scheme described there is more general and can be used for any (over)complete set of projection measurements.

In the standard Pauli basis $\{\sigma_0, \sigma_x, \sigma_y, \sigma_z\}$ the density matrix of the state ρ is given by

$$\rho = \frac{1}{2^n} \sum_{\mu} T_{\mu} \Gamma_{\mu} \quad (7)$$

where $\mu = 1 \dots 4^n$ enumerates all possible n -fold tensor products of Pauli matrices $\Gamma_1 = \sigma_0 \otimes \sigma_0 \otimes \dots \otimes \sigma_0$, $\Gamma_2 = \sigma_0 \otimes \sigma_0 \otimes \dots \otimes \sigma_x$, etc. and with correlations $T_{\mu} = \text{tr}(\rho \Gamma_{\mu})$. To simplify our notation we will use the following mapping for a setting s with a respective outcome r : $(r, s) \rightarrow \nu = 2^{n(s-1)} + r - 1$, hence for the projectors, $M_r^s \rightarrow M_{\nu}$, and for the $A_r^s \rightarrow A_{\nu}$, etc. Then the probabilities to observe a result r for setting s , or ν respectively, are given by

$$P_{\nu} = \text{tr}(\rho M_{\nu}) = \frac{1}{2^n} \sum_{\mu} \text{tr}(M_{\nu} \Gamma_{\mu}) T_{\mu}. \quad (8)$$

Introducing the matrix \hat{B} with elements

$$B_{\nu, \mu} = \frac{1}{2^n} \text{tr}(M_{\nu} \Gamma_{\mu}) \quad (9)$$

Eq. (8) simplifies to

$$\vec{P} = \hat{B} \vec{T}. \quad (10)$$

Inverting Eq. (10), the correlations can be obtained from the probabilities P_{ν} , i.e., $T_{\mu} = \sum_{\nu} (\hat{B}^{-1})_{\mu, \nu} P_{\nu}$. Note that this is possible for any set of measurement operators. In case of a tomographically overcomplete set, i.e. $\nu > \mu$ the inverse \hat{B}^{-1} has to be replaced by the pseudo inverse $\hat{B}^{-1} \rightarrow B^+ = (B^{\dagger} B)^{-1} B^{\dagger}$. Reinserting T_{μ} one obtains

$$\rho = \frac{1}{2^n} \sum_{\nu, \mu} (\hat{B}^{-1})_{\mu, \nu} \Gamma_{\mu} P_{\nu}. \quad (11)$$

For finite data sets, the P_{ν} are replaced by the frequencies f_{ν} and with

$$A_{\nu} = \frac{1}{2^n} \sum_{\mu} (\hat{B}^{-1})_{\mu, \nu} \Gamma_{\mu} \quad (12)$$

Eq. (1) is obtained.

SM 2: Bias for other prominent states

The occurrence of a bias for fidelity estimation based on ML and LS state reconstruction is by no means a special feature of the GHZ state. In Fig. 5 we show some further examples of the corresponding dependencies of the bias on the number of measurements per setting N_s for the W and the fully separable state $|\psi\rangle \propto (|0\rangle + |+\rangle)^{\otimes 4}$. For all these pure states we assume that they are mixed with white noise for an overall initial fidelity of 80%, so that the states are not at the border of the state space.

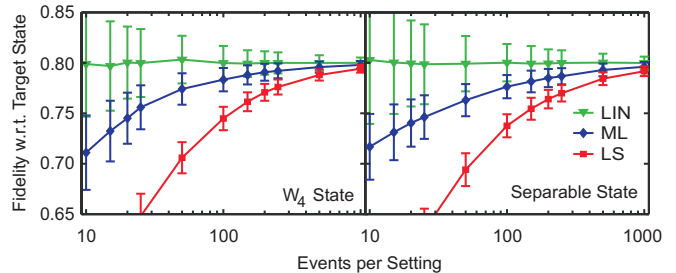


FIG. 5: The behavior of ML, LS and LIN depending on the number of events N_s per setting for different noisy initial states ρ_0 .

Furthermore we observed that the fidelity values as inferred via LS are systematically lower than those obtained using ML, see Fig. 6.

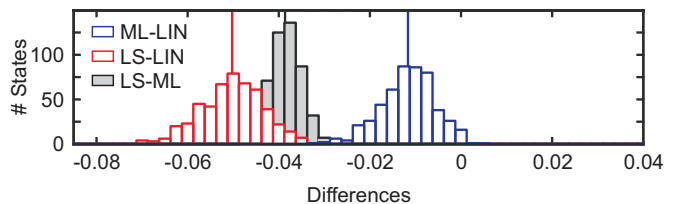


FIG. 6: Here we show the differences of the respective fidelity estimates evaluated for each single simulated tomography experiment as shown in Fig. 1 of the main text. It shows that the respective ML or LS estimate, with one rare exception, is always lower than the LIN estimate. Comparing ML and LS (gray) shows that not only on average but also for every single data set LS delivers a smaller fidelity value than ML.

SM 3: Bootstrapping

As already mentioned in the main text, in many publications where QST is performed the standard error bar is calculated by bootstrapping based on Monte Carlo methods. One can here distinguish between parametric bootstrapping, where $f^{(i)}$ are sampled according to $\hat{P}^s(r) = \text{tr}(\hat{\rho}(f_{\text{obs}}) M_r^s)$, and non-parametric bootstrapping, where $\hat{P}^s(r) = f_{\text{obs}}$ is used instead.

We consider again the four-qubit GHZ state of 80% fidelity and $N_s = 100$. Interpreting the simulations of Fig. 1 as Monte-Carlo simulations from the parametric bootstrap with $\hat{P}^s(r) = \text{tr}(\varrho_0 M_r^s)$ we have already seen that ML and LS yield fidelity estimates below the actual value. If one uses now one of these data sets f_{obs} as a seed to generate new samples $f^{(i)}$ the fidelity decreases further. As shown in Fig. 7 this happens in particular for parametric bootstrapping (0.777 ± 0.011 for ML and 0.700 ± 0.012 for LS) while non-parametric bootstrapping (0.780 ± 0.011 for ML and 0.714 ± 0.012 for LS) weakens this effect. However, in this context, one is interested in fact in the standard deviation of the simulated distribution. In our simulations it is somewhat smaller than the distribution of linearly evaluated fidelities. This means, the biasedness of ML and LS methods leads to a false estimate of the error, too.

SM 4: Confidence regions for states vs. scalar quantities

Let us now comment on confidence regions (CR) for density operators and CR on parameter functions Q . Having a (tractable) method to compute CR for states $\hat{C}_\varrho(f)$ [11], one could think that this region of states also provides good CR for the parameter functions Q , if one manages to evaluate the minimal and maximal values of $Q(\varrho)$ for all $\varrho \in \hat{C}_\varrho(f)$. However, such CR are typically

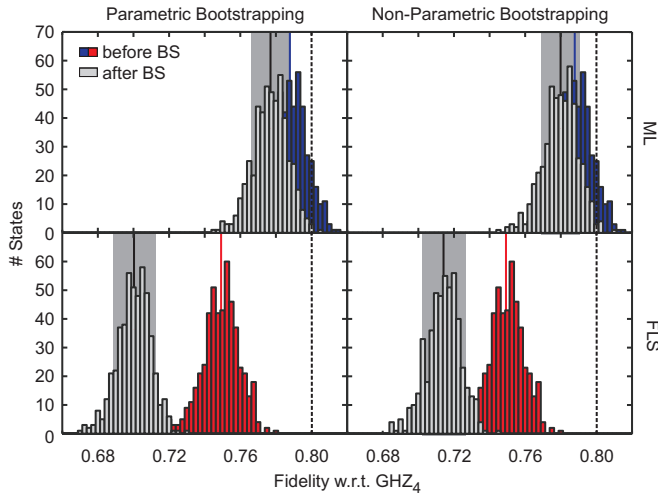


FIG. 7: Error bar computation for the fidelity of the four-qubit GHZ state via Monte-Carlo simulation using either parametric or non-parametric bootstrapping with the data from Fig. 1. For each of these 500 observations f_{obs} , 100 new data sets $f^{(i)}$ were generated and reconstructed in order to deduce the mean and standard deviation as an error bar for the fidelity. The histograms denoted by “after BS” show the distributions of these means together with an averaged error bar given by the gray shaded areas. The initial values for the fidelities are described by the dashed lines.

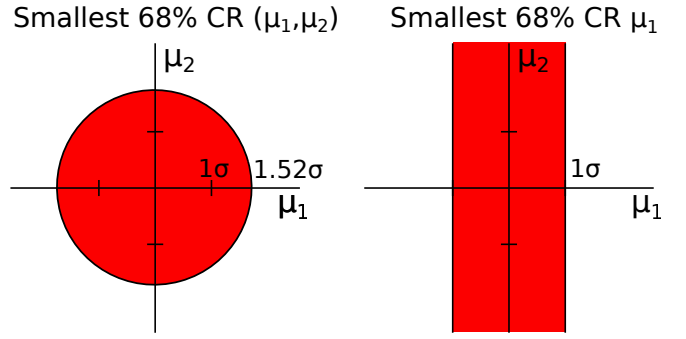


FIG. 8: Which confidence region is the smallest? If one is interested in both mean values $\vec{\mu} = (\mu_1, \mu_2)$ then clearly the left one represents the smallest one, but if $Q(\vec{\mu}) = \mu_1$ is chosen, then the right one is much better than the projected left one.

much worse than CR evaluated for Q directly, the reason being the large freedom in how to build up a CR. Let us give the following illustrative example, see also Fig. 8:

Let us consider the task to obtain a CR for the two mean values $\vec{\mu} = (\mu_1, \mu_2)$ of two independent Gaussian experiments, where the first N samples x_i are drawn from $\mathcal{N}(\mu_1, \sigma^2)$ while the remaining N instances y_i originate from $\mathcal{N}(\mu_2, \sigma^2)$, both with the same known variances. If one is interested in an 68% CR for both mean values $\vec{\mu}$ then both possible recipes

$$\hat{C}^{(1)} = \{\vec{\mu} : \|\vec{\mu} - (\bar{x}, \bar{y})\| \leq 1.52\sigma/\sqrt{N}\}, \quad (13)$$

$$\hat{C}^{(2)} = [\bar{x} - \sigma/\sqrt{N}, \bar{x} + \sigma/\sqrt{N}] \times (-\infty, \infty) \quad (14)$$

with $\bar{x} = \frac{1}{N} \sum_i x_i$ and similar for \bar{y} are valid 68% CR. However, while $\hat{C}^{(1)}$ yields the smallest area for the CR, it gives a much larger confidence region for $Q(\vec{\mu}) = \mu_1$ than if we would directly use $\hat{C}^{(2)}$, which in fact is the smallest one for μ_1 . Note that this effect increases roughly with $\sqrt{\text{dim}}$ if one adds further parameters in the considered Gaussian example. Therefore we see that “error bars” associated with CR on the density operator are not the best choice if one is interested only on a few key properties of the state.

SM 5: Bounds on convex/concave functions

As mentioned in the main text, one can directly bound convex (or concave) functions $g(x)$ by linear ones using an operator L

$$\text{tr}(\varrho_0 L) \leq g(\varrho_0). \quad (15)$$

Here, we want to explain in detail how the operator L can be determined from the derivatives of $g[\varrho(x)]$. Therefore, we parametrize the density operator $\varrho(x) = \mathbb{1}/\text{dim} + \sum_i x_i S_i$ via an orthonormal basis S_i of Hermitian traceless operators. A possible choice for the

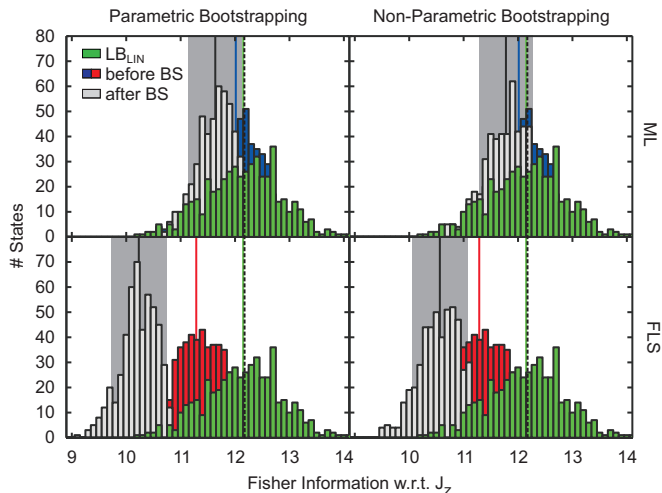


FIG. 9: Full analysis of a Pauli QST scheme with $N_s = 100$ on four qubits in order to deduce the quantum Fisher information with respect to $H = J_z$. As the true underlying state we assume again a noisy four-party GHZ state. We observe that the quantum Fisher information is underestimated from both ML and LS, while the lower bound deduced from LIN is fine.

S_i are all normalized traceless tensor products of the Pauli matrices and the identity. Since we employ an affine parametrization, the function $g(x) = g[\varrho(x)]$ is convex. Direct calculation shows that choosing the operator $L[\varrho(x')] = l_0 \mathbb{1} + \sum_i l_i S_i$ as

$$l_0 = g[\varrho_{\text{guess}}(x')] - \sum_i x'_i \frac{\partial}{\partial x_i} g[\varrho_{\text{guess}}(x')] \quad (16)$$

$$l_i = \frac{\partial}{\partial x_i} g[\varrho_{\text{guess}}(x')] \quad (17)$$

gives due to the convexity condition $g(x) \geq g(x') + \nabla g(x')^T (x - x')$ a lower bound as in Eq. (15). Here, $L[\varrho(x')]$ is computed on a “guess” x' , i.e., $\varrho_{\text{guess}}(x')$ of the true state ϱ_0 . Recall that while the guess ϱ_{guess} must be a valid state the lower bound $\text{tr}(\varrho_0 L)$ is well-defined also for nonphysical density operators.

As an example how to apply this linearization, let us consider the quantum Fisher information $f(x) = F(\varrho, H)$, which measures the suitability of a state ϱ to determine the parameter θ in an evolution $U(\theta, H) = e^{-i\theta H}$. More explicitly the formulae are given by

$$f(x) = 2 \sum_{jk} \frac{(\lambda_j - \lambda_k)^2}{\lambda_j + \lambda_k} H_{jk} H_{kj}, \quad (18)$$

$$\frac{\partial}{\partial x_i} f(x) = 4 \sum_{jkl} \frac{\lambda_j \lambda_k + \lambda_j \lambda_l + \lambda_k \lambda_l - 3\lambda_j^2}{(\lambda_j + \lambda_k)(\lambda_j + \lambda_l)} H_{jk} S_{i,kl} H_{lj} \quad (19)$$

where $\{\lambda_i, |\psi_i\rangle\}$ denotes the eigenspectrum of $\varrho(x)$, $H_{jk} = \langle \psi_j | H | \psi_k \rangle$ and $S_{i,kl} = \langle \psi_k | S_i | \psi_l \rangle$. In order to compute the derivative of the Fisher information one can employ the alternative form, as given for instance in Ref. [26],

$$F(\varrho, H) = \text{tr}[(H\varrho^2 + \varrho^2 H - 2\varrho H \varrho) J_\varrho^{-1}(H)], \quad (20)$$

$$J_\varrho^{-1}(H) = \int_0^\infty dt e^{-t/2\varrho} H e^{-t/2\varrho}. \quad (21)$$

such that the derivative can be computed via the help of matrix derivatives [28].

Now let us imagine that we want to determine the quantum Fisher information of a four-qubit state with respect to $H = J_z$, while our true underlying state ϱ_0 is once more the noisy GHZ state of 80% fidelity. Figure 9 shows the full simulation of a Pauli tomography experiment with $N_s = 100$ together with the standard error analysis using parametric or non-parametric bootstrapping. As with the other examples, we observe a systematic discrepancy between the results of standard QST tools and the true value. In this case, though the quantum Fisher information is typically larger for stronger entangled states, ML or LS underestimate the true capabilities of the state. However, if we use the described method for LIN (with an in this case optimized operator L) the lower bound via LIN is fine.

For completeness, we also give the respective derivatives for further convex functions of interest like the purity $g(x) = \text{tr}(\varrho^2)$

$$\frac{\partial}{\partial x_i} g(x) = 2 \text{tr}[S_i \varrho(x)] \quad (22)$$

and correspondingly for the von Neumann entropy $g(x) = -\text{tr}(\varrho \log \varrho)$

$$\frac{\partial}{\partial x_i} g(x) = -\text{tr}[S_i (\log \varrho(x) - \mathbb{1})]. \quad (23)$$